

Shrinking \hbar as a recipe for revealing classical-like contributions in optical potential cross sections

R. Anni

*Dipartimento di Fisica dell'Università, Università di Lecce, Lecce, Italy
Istituto Nazionale di Fisica Nucleare, Sezione di Lecce, Lecce, Italy*

A simple recipe for revealing classical-like contributions in optical potential cross sections is proposed. The recipe is based on the fact that the classical-like properties are not expected to depend on the actual value of \hbar . This allows us to identify the classical-like characteristics of an optical potential cross section by simply repeating the calculation with different values of \hbar , and observing which properties of the cross section are invariant. This method is applied to the cross sections of a few optical potentials used to describe the recent data of light heavy-ion elastic scattering.

I. INTRODUCTION

The recent detailed measurement of the elastic differential cross sections of light heavy-ions [1–4] have stimulated a revival of the interest in heavy-ion elastic scattering as a useful tool to obtain a better understanding of nuclear properties.

Deep real parts and shallow imaginary ones characterise the optical potentials used to reproduce these experimental cross sections. The reduced absorption, that seems necessary to reproduce the observed data, makes the cross section sensitive to contributions coming from the internal region of the interaction, allowing the study of the interaction properties in regions where the densities of the two nuclei strongly overlap.

The number of partial waves that contribute to these optical potential cross sections is in all these cases rather large. This allows one to hope that semiclassical techniques can be used to connect the behavior of the cross sections, in certain angular ranges, to the properties of the interaction, in some corresponding spatial region.

The recognition of the presence of classical-like contributions in an experimental cross section may be a very difficult job, but at least in principle, their determination in an optical potential cross section should be easier. Here the problem is in fact reduced to performing a semiclassical analysis of the optical potential cross section.

The classical limit of scattering by a real potential is well understood since more than forty years [5]. This limit is found with the use of asymptotic approximations for the scattering function $S(\lambda)$ ($\lambda = l + \frac{1}{2}$), for the Legendre polynomials $P_l(\cos\theta)$, and for the partial wave expansion of the scattering amplitude $f(\theta)$. As a result one obtains that $f(\theta)$ can be expressed in terms of one, or more, stationary phase contributions. The square modulus of each stationary phase contribution exactly coincides with a corresponding contribution from one branch of the classical deflection function. Because each stationary point contribution has also a phase, if two or more stationary points contribute to $f(\theta)$ in some

angular range, oscillations appear in the cross section arising from interference. These oscillations disappear in the classical limit by averaging over the finite resolution of the experimental devices.

Unfortunately this simple scheme cannot, in general, be applied to the optical potentials commonly used to describe the elastic scattering of two heavy-ions. In the scattering process from the optical potentials currently used (also neglecting the complications arising from the presence in the interaction of an imaginary part) the classical integral actions, in units of \hbar , are large but not infinite and quantum contributions, superimposed to classical-like ones, survive in the scattering function and in the corresponding cross section. Only in the extreme classical limit these quantum contributions are expected to disappear, remaining confined in regions whose width go to zero.

Several semiclassical methods [6] were developed to extend the range of application of the classical description to the dynamical regions in which an imaginary part is present in the potential and the extreme classical conditions are not fully satisfied.

These methods considerably extend the possibility of describing the semiclassical properties of a scattering process. However, presently, they predict cross sections in good quantitative agreement with the exactly calculated ones only in certain energy ranges, depending on the optical potential considered.

Furthermore, also admitting that we are within the range of validity of some of the available semiclassical methods, their application to practical cases is slightly more difficult, and much less popular, than the direct calculation of the exact cross section. Owing to this, one could ask if some trick exists, which is able to provide quickly a useful indication on the classical-like nature of some properties of a cross section, without worrying about the complications of the semiclassical techniques and about their ranges of validity.

In this paper one of these possible tricks is investigated. The base idea is that the classical-like properties

must not depend on \hbar . Owing to this all the properties of a cross section which do not depend on the value which is attributed to \hbar , in the framework of a quantum calculation, can be considered of classical origin.

The main ingredients of this simple recipe, which can be easily implemented in any standard optical potential code, are presented in Sect. II. In order to test the method in a simple case, in Sect. III we present the results obtained for a real optical potential. In Sect. IV and V the method is applied to analyze the behavior of two optical potential cross sections, fitted to the experimental data of $^{16}\text{O} + ^{12}\text{C}$ at the laboratory energies of 132 and 200 MeV [4].

For the cases considered, the results of the quantum calculation are first compared with the corresponding classical ones. This comparison is not really necessary for the application of the recipe and is introduced here only to show the reliability of the method to identify correctly classical-like properties.

The results obtained are that the qualitative behavior of the optical potential cross sections smoothly changes with varying \hbar . Considering the oscillations which appear in the cross section as arising from the interference between simpler amplitudes, one observes that with decreasing values of \hbar some of these amplitudes continue to modify their behavior, contributing to angular ranges of decreasing width, while others become insensitive on any further decrease of \hbar . The former reveal their quantum origin, the latter their classical nature.

The comparison of the behavior of the real cross section (calculated with the true value of \hbar) with that of the fictitious cross sections (calculated attributing to \hbar values sufficiently small) allows one to obtain easy indications on the classical-like properties of the true cross section.

II. MAIN INGREDIENTS OF THE RECIPE

Accordingly to classical mechanics, the cross section for scattering from a potential $V(r)$ is completely determined by the deflection function

$$\Theta(\lambda) = \pi - 2 \int_{r_0}^{\infty} \frac{\lambda}{kr^2 \sqrt{1 - \frac{V(r)}{E} - \frac{\lambda^2}{k^2 r^2}}} dr, \quad (1)$$

where $L = \lambda\hbar$ and $p = k\hbar$ are, respectively, the angular and linear momenta, and r_0 is the turning point which delimitates from below the classically accessible region of the radial motion.

The deflection angle $\Theta(\lambda)$ is connected to the scattering angle $\theta(\lambda)$ through the relation

$$\theta(\lambda) = \arccos[\cos \Theta(\lambda)]. \quad (2)$$

Remembering that $\Theta(\lambda) \rightarrow 0$ for $\lambda \rightarrow \infty$, if $\Theta(\lambda)$ is a monotonous function and $|\Theta(\lambda)| < \pi$, the differential cross section is given by

$$\sigma(\theta) = \frac{\lambda(\theta)}{k^2 \sin \theta} \left| \frac{d\lambda(\theta)}{d\theta} \right|, \quad (3)$$

where $\lambda(\theta)$ is the inverse function of $\theta(\lambda)$.

If the above conditions are not satisfied, particles with different angular momenta can be scattered at the same scattering angle. This happens when critical λ values exist at which the deflection function has maxima or minima, or crosses the values $-m\pi$, $m = 0, 1, \dots$. In this case $\theta(\lambda)$ can be inverted only within intervals limited by two consecutive critical λ values, corresponding to different branches of the deflection function, and the cross section is given by

$$\sigma(\theta) = \sum_j \frac{\lambda_j(\theta)}{k^2 \sin \theta} \left| \frac{d\lambda_j(\theta)}{d\theta} \right|, \quad (4)$$

where the sum runs over all the branches of the deflection function containing a deflection angle corresponding to the scattering angle θ .

Accordingly to quantum mechanics, the cross section for scattering from a potential $V(r)$ is completely determined by the scattering function $S(\lambda)$. This quantity defines the scattering amplitude

$$f(\theta) = \frac{i}{k} \sum_{l=0}^{\infty} \lambda [1 - S(\lambda)] P_{\lambda - \frac{1}{2}}(\cos \theta), \quad (5)$$

and the cross section $\sigma(\theta)$, which is the square modulus of $f(\theta)$.

The classical limit of the quantum cross section is realized through the appearance of a link between $S(\lambda)$ and $\Theta(\lambda)$. These two quantities are in fact connected by the relation

$$\lim_{\hbar \rightarrow 0} \frac{d \arg S(\lambda)}{d\lambda} = \Theta(\lambda). \quad (6)$$

Thanks to this link, the classical mechanics expression for the cross section is recovered using the asymptotic expansion for the Legendre polynomials, transforming the partial wave expansion into a sum of integrals, and evaluating asymptotically these integrals using the stationary phase method.

The properties of the deflection function fix the number of the stationary phase points which contribute to $f(\theta)$ at each angle. The contribution from each stationary phase

¹The appearance of \hbar does not imply the use of quantum mechanics, but only the choice of convenient units.

point has a modulus, whose square just coincides with the classical expression, and a phase. The phase factors produce an oscillatory behavior in the cross section in the angular regions where two, or more, stationary phase points contribute, and the classical result is finally obtained only after averaging over these oscillations, whose period goes to 0 in the classical limit, to account for the finite resolution of the experimental devices.

Owing to this, a signature of the contribution of classical-like trajectories is the presence in the angular distribution of angular intervals in which the cross section, changing the value attributed to \hbar , either does not change or, if it changes, keeps as upper and lower envelopes the curves corresponding to the maximal constructive and destructive interference amongst all the contributions from the different branches of the deflection function. In the following these envelopes and the delimited region will be named *interference limits* and *interference region*, respectively.

The interference limits can be calculated starting from the properties of $\Theta(\lambda)$, or they can be found by performing a quantum mechanics calculation by attributing to \hbar different values, sufficiently smaller than the physical value.

This scheme is well suited to bring out classical like-contributions in the cross section for scattering by a real potential, but it cannot be directly applied to the cases in which an imaginary part is introduced in the interaction to simulate the effects of the population of channels different from the elastic one.

The imaginary part $W(r)$ of the potential removes flux from the elastic channel and the time dependence of the probability density, $\rho(\mathbf{r}, t) = |\psi(\mathbf{r}, t)|^2$, of finding the scattering partners at time t at a relative position \mathbf{r} satisfies the equation [7]

$$\frac{\partial \rho(\mathbf{r}, t)}{\partial t} + \text{div} \mathbf{j}(\mathbf{r}, t) = -\frac{2W(r)}{\hbar} \rho(\mathbf{r}, t), \quad (7)$$

where $\mathbf{j}(\mathbf{r}, t)$ is the probability current density. The above equation suggests the interpretation of the quantity $w = 2W(r)/\hbar$ as the probability per unit of time for a transition out of the elastic channel.

With this interpretation of w the form of the classical cross section given by Eq. 4 remains the same, apart for the introduction, in each term on the r.h.s, of a multiplicative factor

$$P(\lambda) = \exp \left(-\frac{1}{2\hbar} \int_{r_0}^{\infty} \frac{\frac{W(r)}{E}}{\sqrt{1 - \frac{V(r)}{E} - \frac{\lambda^2}{k^2 r^2}}} dr \right), \quad (8)$$

expressing the probability that the particles with angular momentum $\lambda\hbar$ are not removed from the elastic channel during their motion along the classical trajectory.

We note, in passing, that this form for the cross section is just that obtained using the naive WKB approximation [8] to estimate $S(\lambda)$, and the stationary phase

method to evaluate $f(\theta)$. Within this scheme the probability that the particles with angular momentum $\lambda\hbar$ are not removed from the elastic channel can be identified with $|S(\lambda)|^2$, which has exactly the dependence from the imaginary part of the potential deriving from the above classical interpretation.

In accordance with this picture, in the search process of the interference limits based on the variation of the value attributed to \hbar (in order to keep constant the survival probability factor) the imaginary potential must be scaled with the same factor used for \hbar . This will be the additional caution used to look for traces of classical-like contributions in the quantum mechanics cross section.

Apart from in the cross section, traces of classical-like contributions can also be found in the behavior of $|S(\lambda)|$ and of $d \arg S(\lambda)/d\lambda$. In the following this last quantity will be named *quantum deflection function* and indicated with $\Theta_Q(\lambda)$.

If the classical limit is well approached both $|S(\lambda)|$ and $\Theta_Q(\lambda)$ are expected not to depend on the value of \hbar , if plotted versus the impact parameter $b = \lambda/k$.

The conventional optical potential codes provide the values of $S(\lambda)$ for half integer positive λ values. These values can be used directly to plot $|S(\lambda)|$ versus the impact parameter b , and using the finite difference formula

$$\Theta_Q(\lambda) = \frac{d \arg S(\lambda)}{d\lambda} \simeq \frac{\arg S(\lambda + \Delta\lambda) - \arg S(\lambda - \Delta\lambda)}{2\Delta\lambda}, \quad (9)$$

with $\Delta\lambda = \frac{1}{2}$, they often also provide a reasonable approximation for $\Theta_Q(\lambda)$ at integer λ values. In the cases here considered, for a very few l values, this simple approximation provides a bad estimate for $\Theta_Q(\lambda)$. This happens when the true variation of $\arg S(\lambda)$, between consecutive integer l values, becomes larger than π . It is due to the fact that, in the optical code that we use, the arguments of $S(\lambda)$ are defined modulus 2π and the angle α between two successive $S(\lambda)$ values, in the complex Argand plane, is taken as the convex one. Only for an extreme precaution, in the present work, the quantity $\Theta_Q(\lambda)$ was estimated, outside our conventional optical code, using Eq. 9 with a step $\Delta\lambda = 0.1$ for $\alpha > \frac{\pi}{4}$ and of 0.5 elsewhere.

The fact that the values of $|S(\lambda)|$ and $\Theta_Q(\lambda)$, calculated with different values of \hbar and plotted against b , lie on the same curve can be considered a signature of the dominance of a classical-like mechanism in the scattering process. However this fact, alone, does not guarantee that the cross section also closely follows the behavior predicted by the classical mechanism. The realization of the classical limit for the cross section also requires that the integrals, in which the partial wave expansion of $f(\theta)$ is transformed, can be approximated by the stationary phase method and that, at the stationary phase points, the Legendre functions are well approximated by their non-uniform asymptotic expansions.

It is well known that the stationary phase method fails in a neighbourhood of the classical rainbow angles and that the uniform method allows an estimation of the contributions from the stationary points in terms of Airy functions. The uniform approximation substitutes the singularity of the classical cross section, followed by the sharp shadow region, with a maximum in the lit region followed by a decrease of the cross section. In the approach to the classical limit the maximum moves towards the rainbow angle, and the cross section very rapidly decreases in the shadow region. Therefore in general deviations are expected between the behavior of the quantum and the classical cross sections around the classical rainbow scattering angles.

Deviations are also expected in the extreme backward direction where the usual non-uniform approximation for the Legendre functions does not hold. This approximation is responsible for the presence of the factor $1/\sin\theta$ in the classical limit of the cross section and, consequently, for the appearance of the classical glory singularity.

These types of deviations, thypical of quantum effects, are however standard and one can easily recognize their presence in the search process of classical-like properties of the cross sections.

III. REAL OPTICAL POTENTIAL CROSS SECTION

To test the effectiveness of the method based on the variation of \hbar , we first consider the cross section of a fictitious real optical potential having a conventional Woods-Saxon form factor with parameters $V_0 = 282.2$ MeV, $R_v = 2.818$ fm and $d_v = 0.978$ fm. This potential is the real part of one of those used for fitting the elastic scattering cross section of $^{16}\text{O} + ^{12}\text{C}$ at $E_{\text{Lab}} = 132$ MeV [4]. For all the cases here considered, the Coulomb part of the interaction is described using an analytical potential that closely approximates the Coulomb potential of two uniformly charged spheres with radii of 3.54 fm and 3.17 fm.

A. Comparison with the classical cross section

The thick solid line in Fig. 1 shows the classical deflection function $\Theta(\lambda)$, as a function of the impact parameter b . This line, as similar ones for the other cases considered, shows the cubic spline interpolation of the $\Theta(\lambda)$ values calculated at $b = \lambda/k$, with a step $\Delta\lambda = 0.25$, starting from $\lambda = 0$. The open dots in Fig. 1 show the values of $\Theta_Q(\lambda)$ estimated by using Eq. 9 at integer λ values, and the thin curve gives the cubic spline interpolation of the calculated points.

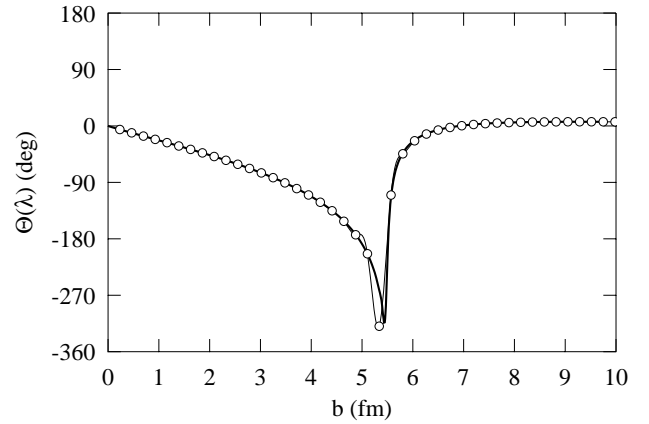


FIG. 1. The thick curve shows the classical deflection function. The open dots represent the values of the quantum deflection function calculated at integer $\lambda = bk$ values. The thin curve shows the cubic spline interpolation of the open dots.

The agreement between the dots and the thick curve is impressive and the small differences between the thin and the thick lines may be a consequence of the method used to interpolate the dots.

The classical deflection function shows a maximum of about 7° at $b_C \simeq 9.3$ ($\lambda_C \simeq 40.2$) and a minimum of about -310° at $b_n \simeq 5.4$ ($\lambda_n \simeq 23.5$). In the classical cross section we therefore expect two rainbow singularities at the scattering angles $\theta_C \simeq 7^\circ$ (Coulomb rainbow) and $\theta_n \simeq 50^\circ$ (nuclear rainbow).

Six different branches of $\Theta(\lambda)$ contribute to the cross section, four corresponding to trajectories coming from the scattering half plane containing the scattering angle (near-side trajectories) and two coming from the opposite half plane (far-side trajectories).

At $b \neq 0$, the deflection function $\Theta(\lambda)$ crosses three times values for which $\sin\theta = 0$. Two glory singularities are expected at $\theta = 180^\circ$ and one, additional to the Coulomb singularity, at $\theta = 0^\circ$.

In the panel (a) of Fig.2 the thick line shows the ratio of the classical mechanics cross section to the Rutherford one. The thin solid and dashed lines give the contributions to the same quantity from the different branches, near- and far-side respectively, of the deflection function.

The appearance of the rainbow singularities are manifest, as are the glory singularities corresponding to the crossing of the deflection function of the -180° deflection angle. The glory corresponding to the crossing of the 0° deflection angle is masked by the Rutherford cross section higher order singularity at the same scattering angle.

In the semiclassical limit a phase factor is associated to each contribution from the different branches of the deflection function. In the panel (b) of Fig. 2 the thin solid lines show the interference limits of these contributions, while the thick dashed and solid lines give, respectively, the classical and the quantum cross sections.

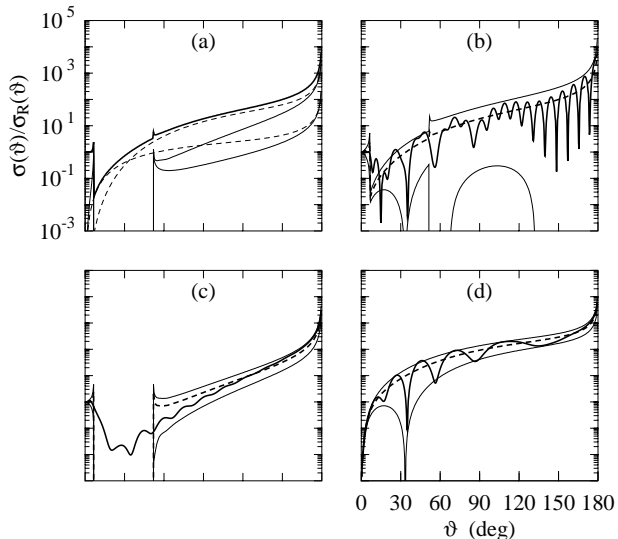


FIG. 2. (a) Classical cross section (thick line), near- (thin solid lines) and far-side (thin dashed lines) contributions to the classical cross section; (b) quantum (thick solid line) and classical (thick dashed line) cross sections, the thin lines show the interference limits; (c) the same as in panel (b) for the near-side cross sections; (d) the same as in panel (b) for the far-side cross sections.

With the exclusion of a small angular range at the right of θ_C , the oscillations appearing in the quantum cross section are well within the interference region. The interference limits cannot, however, be considered the upper and lower envelopes of the quantum cross section. The reason for this is clarified in the panels (c) and (d) of the same figure, where the thick solid and dashed lines show the near- and far-side components of the quantum [9] and classical cross sections, respectively. The interference limits of the classical far-side cross section are almost perfect envelopes of the quantum far-side cross section. The period of the oscillations of this cross section decreases with the increase of the scattering angle, which corresponds to a decrease of the deflection angle. This tendency is confirmed by the very long period of the oscillation appearing in the backward angles near-side cross section. Owing to this, the oscillations can be interpreted as arising from interference of classical-like trajectories whose phase differences tend to decrease while approaching the nuclear rainbow angular momentum. In the present case, these phase differences are too small to allow us to observe the maximal constructive and destructive interference amongst all the four branches of the deflection function contributing to angles larger than θ_n .

In the classical near-side cross section a dark region is present between θ_C and θ_n . From both the shadow boundaries, this dark region appears partially enlightened by the quantum near-side cross section, and the tails of the two shadows overlap with each other producing some interference. The shadow contribution to the right of θ_C decreases rather rapidly. This makes difficult

to justify, as arising from this contribution, the persistence of the interference pattern in the near-side cross section at angles larger than about 30° . In this angular range, the oscillations suggest the existence of an additional non-classical contribution.

The near- and far-side cross section interference patterns are considerably simpler than the full cross section one. This complicate interference pattern of the full cross section arises from the coherent superposition of the simpler far- and near-side amplitudes. It is the folding of the plane of Fig. 1, necessary to obtain the dependence of the scattering angle from the impact parameter, which is responsible for this complicate interference pattern. The near- and far-side decomposition allow one to unfold the quantum cross section, considering its dependence on the deflection angle rather than on the scattering angle. In Fig. 3 the thick solid line shows this unfolded cross section. In order to eliminate the appearance of the glory singularities in the classical cross sections, in this figure the cross sections multiplied by $\sin \theta$ are plotted.

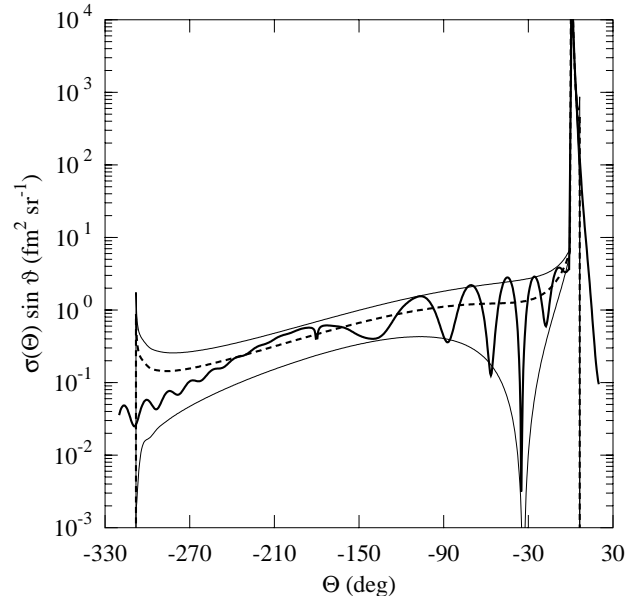


FIG. 3. Unfolded quantum (thick solid line) and classical (thick dashed line) cross sections, and classical interference limits (thin lines), plotted versus the deflection angle.

The unfolded quantum curve shows an irregular behavior in a small angular interval around -180° . This irregular behavior is probably due to the fact that the singularities of the quantum near- and far-side cross sections at 180° are slightly different from the $1/\sin \theta$ singularity predicted by the non-uniform approximation of the Legendre functions.

With the exclusion of this small interval, one can however appreciate the attempt of the near-side curve ($\Theta < -180^\circ$) to match continuously the far-side one ($-180^\circ < \Theta < 0^\circ$).

The comparison of $\Theta_Q(\lambda)$ with $\Theta(\lambda)$, and of the quan-

tum cross sections (full, near- and far-side) with the corresponding classical ones, allows one to recognize the presence, in the quantum quantities, of contributions which are very close to those expected from classical-like trajectories.

A nice Airy-like pattern appears in the unfolded quantum cross section. The increase of the period of the main oscillations, with decreasing the deflection angle, well justifies the fact that the interference limits are rather far from representing the envelopes of the full quantum cross section.

B. Pure quantum mechanical analysis

The comparison of the classical and quantum cross sections allows one to derive clear evidences of classical-like characteristics in the quantum cross section. The same result can be obtained without using any classical mechanics calculation, by simply observing the changes produced in the scattering function and in the cross section by changing the value attributed to \hbar .

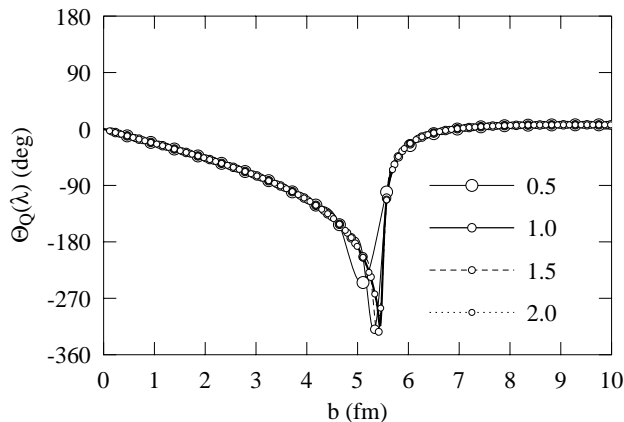


FIG. 4. The open dots represent the values of the quantum deflection functions calculated, at integer $\lambda = bk$ values, for the 4 values of the \hbar reduction factor given in the figure. The thin curves show the cubic spline interpolations of the dots and the thick curve show the classical deflection function.

In Fig. 4 the open dots show the values of $\Theta_Q(\lambda)$ calculated at integer λ values using Eq. 9 and substituting \hbar in an optical potential code with $\hbar_f = \hbar/f$, with $f = 0.5, 1.0, 1.5, 2.0$.

Because the spacing in b of points corresponding to an increment of one unit in l is proportional to $1/f$, the abscissae of the points corresponding to $\Delta l = 1, 2, 4$ for the cases $f = 0.5, 1.0, 2.0$ are trivially the same at appropriate b values (the b value corresponding to $\lambda = 1$ for $f = 0.5$ is the same as that corresponding to $\lambda = 2$ for $f = 1.0$ and to $\lambda = 4$ for $f = 2.0$, and so on). In Fig. 4 the open dots corresponding to these values of f result perfectly concentric at the common b values, with the

exclusion of a small range around $b \simeq 5.5$. This provides a striking confirmation of the classical scale invariance properties of $\Theta_Q(\lambda)$ for almost all the values of the angular momentum.

The thick solid curve, representing $\Theta(\lambda)$, shows that also in the above small range, and in the more unfavorable case ($f = 0.5$, \hbar two times larger), the agreement between $\Theta_Q(\lambda)$ and $\Theta(\lambda)$ is rather good. This agreement becomes practically perfect for the most favorable case ($f = 2.0$, \hbar two times smaller).

The tendency of all the $\Theta_Q(\lambda)$ points (plotted against b for different \hbar values) to lie on the same curve is a clear signature of the dominance of the classical dynamics in the determination of the properties of $S(\lambda)$. This allows one to obtain information on the classical properties of $S(\lambda)$ using only quantities calculated by a conventional optical potential code, and the direct calculation of the classical deflection function is not really necessary.

In Figs. 5, 6 and 7 are shown the full, near- and far-side cross sections, respectively, calculated with the values of the reducing factor f given in the figures.

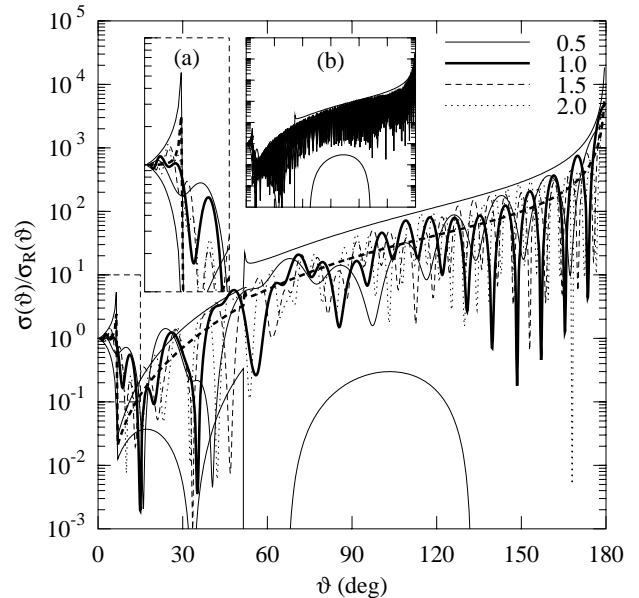


FIG. 5. Quantum cross sections for the 4 value of the \hbar reduction factor given in the figure. The thick dashed and thin solid curves show, respectively, the classical cross section and the interference limits. The inset (a) gives an enlargement of the rectangular area of the figure limited by the dashed lines. The inset (b) gives a reduction of the whole area of the figure. In the inset (b) are plotted the quantum, the classical cross sections and the interference limits together with the quantum cross sections calculated with values of the reduction factor from 3 to 4.

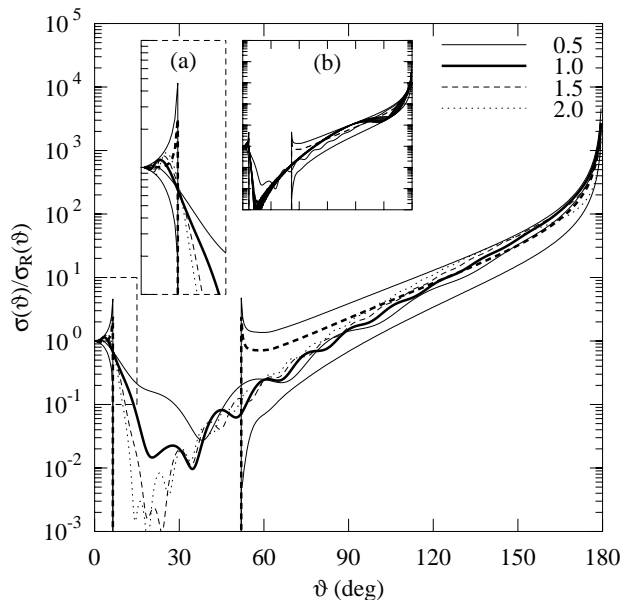


FIG. 6. The same as Fig. 5 for the near-side cross sections

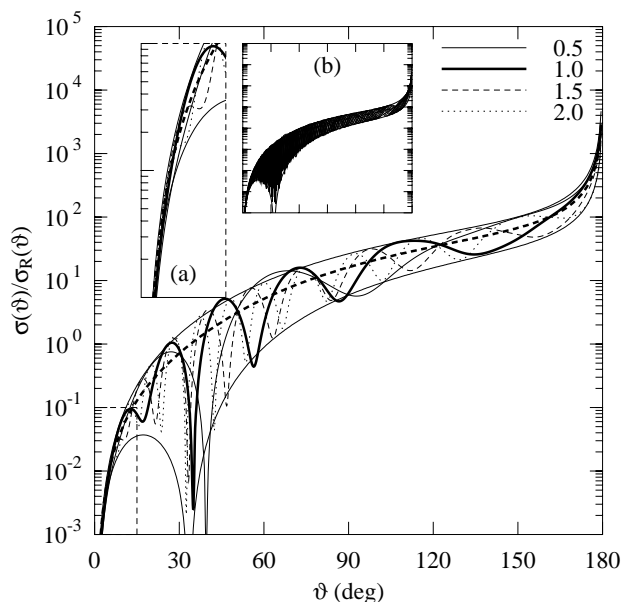


FIG. 7. The same as Fig. 5 for the far-side cross sections

In these figures the thick dashed and thin solid lines show the classical cross sections and their interference limits, respectively. These lines were drawn only to remember these classical limits. As for the deflection function, the drawing of these classical quantities is not necessary to recognize the presence of classical-like contributions.

In all these figures the insets (a) show an enlargement, by a factor 2, of the rectangular regions delimited by the dashed lines, and the insets (b) show a reduction, by a factor 3, of the complete figures. In the insets (b) are plotted the true cross sections together with eleven cross

sections calculated with values of f ranging from 3.0 to 4.0 with a step of 0.1.

By looking at Fig. 5 one observes a rather complicated behavior of the cross sections corresponding to the four values of f considered. This makes it difficult to imagine that the oscillations tend to be confined within well defined regions. This tendency begins to appear in the inset (b), where a rather well defined upper envelope can be observed, and also indications of a lower envelope are present. One explanation of the minor definiteness of the lower envelope can be found in the fact that, with the scale used, the minima are much narrower than the maxima. Using a fixed grid to tabulate the cross section it is more probable to miss a minimum rather than a maximum.

In the angular region delimited by θ_C and θ_n , the full cross sections calculated with the four values of f is in disagreement with the interference limits, particularly in the region to the right of θ_C . This disagreement decreases rapidly with increasing f .

The reason of this behavior is understood by considering Fig. 6, where the near-side cross sections are plotted. In the classical shadow region, by increasing f , the cross sections decrease very rapidly moving to the right of θ_C , while they decrease slowly moving to the left of θ_n . In the inset (b) one can observe that even for f values ranging from 3.0 to 4.0 the decrease of the near-side cross section is slow, moving from the right towards the shadow region. The eleven cross sections only begin to fill gradually the region defined by the interference limits. The phase difference between the classical-like trajectories, which contribute to this part of the near-side cross section, depend weakly on the angle and only a few oscillations appear in the cross section at the maximum value of f considered.

In the treatment of the scattering amplitude using the uniform method around a rainbow angle, the rapidity of the decrease of the cross section, in the classical shadow region, depends on the second derivative of the deflection function at the rainbow angular momentum. The curvature of the deflection function is much higher at the nuclear than at the Coulomb rainbow, and this explains why the two slopes are so different.

Comparing the inset (a) of Fig. 6 with the corresponding inset of Fig. 5, one can also observe that the interference pattern of the near-side cross section, around θ_C , is considerably simpler than that of the full cross section. The additional oscillations in the full cross section arise from the contributions from the far-side amplitude.

The full and the near-side cross sections do not clearly exhibit properties which are invariant with respect to the value attributed to \hbar . This is not the case for the far-side cross sections which are given in Fig. 7. The existence of common upper and lower envelopes for these cross sections is rather well indicated already by the f values ranging from 0.5 to 2.0, and is clearly proved by the f values from 3.0 to 4.0 given in the inset (b) of the figure. Apart from a small distortion of at least one of the two interfering amplitudes this figure provides a strong indication

of the dominance of the contributions from classical-like trajectories already from the value $f = 0.5$ (\hbar two times larger).

IV. COMPLEX OPTICAL POTENTIAL CROSS SECTION: $E_{\text{LAB}} = 132$ MEV

The first complex optical potential considered is one of the potentials whose cross section fits the experimental data at $E_{\text{Lab}} = 132$ MeV [4]. The imaginary part of the potential has a conventional Woods-Saxon form factor with parameters $W_0 = 13.86$ MeV, $R_w = 5.6894$ fm, and $d_w = 0.656$ fm. Its real part is that of the real optical potential previously considered.

This case was chosen because a recent semiclassical analysis [10], using the Brink and Takigawa [11] approximation, has shown that the oscillations appearing in the far-side cross section can be explained as arising from the interference between far-side contributions from the first two terms of the multireflection expansion of the semiclassical scattering amplitude². Because the far-side contribution to the barrier term is responsible for the appearance of the Fraunhofer-like pattern in the barrier cross section, one is naturally induced to think that this contribution should be considered of diffractive nature, i.e. of quantum origin.

It seems therefore interesting to test if the simple recipe here proposed is able to discover the non-classical origin of this contribution. By decreasing the value of \hbar and approaching the classical mechanics limit, one should also observe how this diffractive contribution becomes a classical one.

A. Comparison with the classical cross section

According to the above classical interpretation of the imaginary part of the potential, the presence of this term does not modify the classical deflection function $\Theta(\lambda)$. The imaginary part only introduces a probability $P(\lambda)$ of survival in the elastic channel for particles with angular momentum $\lambda\hbar$.

In the panels (a) and (b) of Fig. 8 the thick lines show, respectively, the square root of $P(\lambda)$ and $\Theta(\lambda)$ as functions of the impact parameter b .

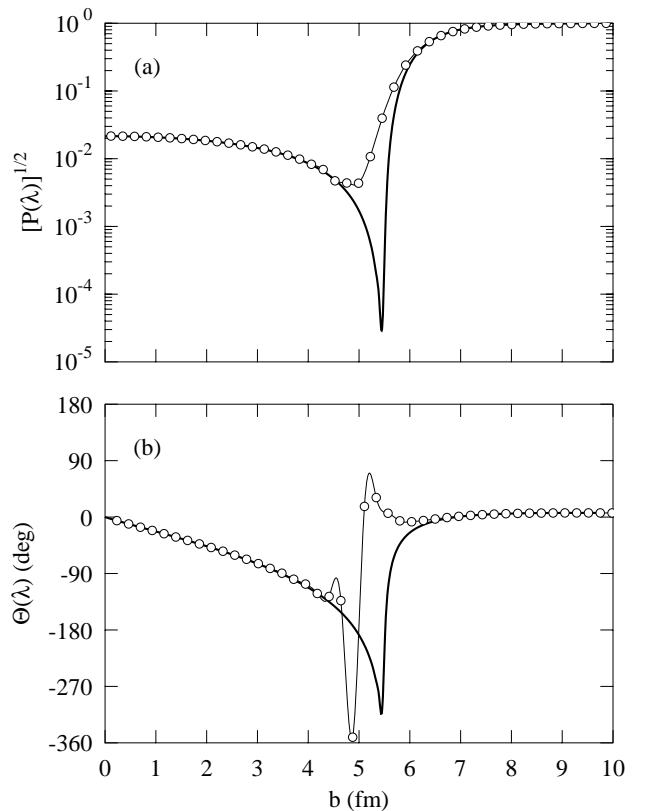


FIG. 8. The thick curves show the classical deflection function (panel (b)) and the square root of the survival probability (panel (a)). The open dots represent the values of the quantum deflection function and of the modulus of the scattering function, calculated at integer and half integer $\lambda = bk$ values, respectively.

In the same figure the dots represent the values of $|S(\lambda)|$ and of $\Theta_Q(\lambda)$ ³ and the thin lines are cubic spline interpolations of the calculated values. The figure shows that the quantum and classical corresponding quantities are in good agreement, apart from a neighborhood around $b \simeq 5$ fm of half width of about 1 fm. The impact parameter value b_n of the nuclear rainbow is in this region, and its position is very close to the position of the deep minimum of $P(\lambda)$. The behavior of $S(\lambda)$ in this region is considerably different from what would be expected in the extreme classical limit. This suggests the dominance of a scattering mechanism different from the

²In the following, the first two terms of the multireflection expansion of the Brink and Takigawa scattering function will be named, respectively, *barrier* and *internal* terms. This terminology, which is rather common in the literature, will be adopted for simplicity, in spite of the presence of contributions from the internal part of the interaction also in the higher order terms of the multireflection expansion.

classical one for particles with angular momenta corresponding to this range of impact parameter values.

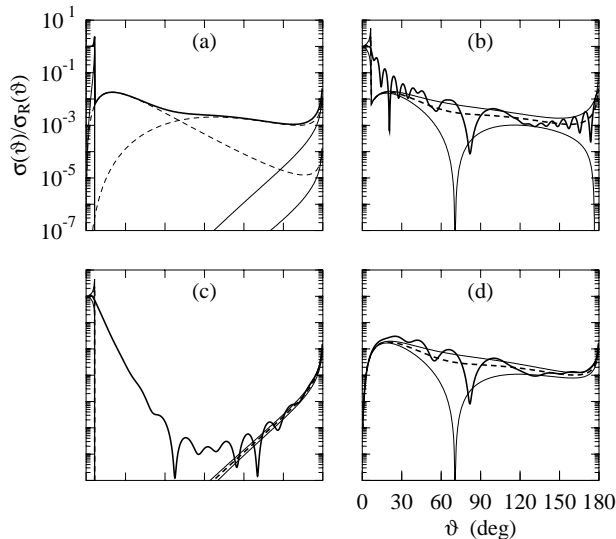


FIG. 9. The same as Fig. 2 for the complex optical potential at $E_{\text{Lab}} = 132$ MeV.

In the different panels of Fig. 9 are shown the same quantities given in the corresponding panels of Fig. 2 for the real potential. At angles larger than θ_C the contributions from all the branches of the deflection function are strongly reduced by the absorption. Each point of the old curves is lowered by the corresponding value of $P(\lambda)$. Furthermore, the deep minimum of $P(\lambda)$, around b_n , produces a dramatic reduction of the contribution from the near-side trajectories with $b \simeq b_n$. Only part of the near-side contributions from the corresponding two branches of $\Theta(\lambda)$ (the two thin solid lines in the right bottom corner of panel (a)) can be observed within the range of the vertical axis of Fig. 9. At backward angles these curves are close to the dashed lines representing the far-side contributions, but they drop very rapidly with decreasing angle going out from the plotted area. The very small values of these contributions at angles just above θ_n prevent the observation of effects in the classical cross section deriving from the nuclear rainbow singularity.

The rapid decrease of these contributions, together with the modifications of the slopes of the contributions from the far-side trajectories, considerably shrinks the

width of the interference region. The borders of this region are shown by the thin lines in the panel (b) of Fig. 9. In the same panel, the thick curve shows the quantum cross section. This curve, in the forward hemisphere, substantially violates the boundaries fixed by the interference limits.

In the panel (c) we show that the violation of the interference limits is mainly due to a violation of the corresponding limits by the near-side component of the full cross section. At angles to the right of θ_C the quantum curve decreases almost exponentially, at the rate of about one order of magnitude per 10° , filling the classical shadow region between θ_C and θ_n . By increasing the angle, oscillations of increasing amplitudes appear, indicating the interference of the exponentially decreasing contribution with another one.

In the backward hemisphere, decreasing the angle below 180° , the quantum near-side curve initially follows the classical one, then it begins to show oscillations with an amplitude increasing with decreasing angle. These oscillations can be interpreted as arising from the interference of a classical-like contribution with a different contribution, of non-classical origin. This additional contribution appears to be the same producing the oscillations in the exponential tail at the right of θ_C .

This behavior is qualitatively similar to that observed in the near-side cross section of the real potential. The only difference is represented by the fact that now the curves at the right of θ_n are downward shifted and decrease more rapidly by decreasing the angle. This allows one to observe in a wider angular range the exponential decrease at the right of θ_C .

The quantum and classical far-side cross sections given in the panel (d) show that a relevant contribution to the violation of the classical interference limits comes also from at least one of the two terms responsible for the oscillatory pattern of the quantum far-side cross section. This confirms the results obtained with the semiclassical analysis [10], suggesting that one of these contributions is not of classical origin.

B. Pure quantum analysis

The panels (a) and (b) of Fig. 10 show, respectively, $|S(\lambda)|$ and $\Theta_Q(\lambda)$ for the four values of f given in the

³The quantum deflection function shown in Fig. 1 of Ref. [10] was obtained by using for all the λ values an increment $\Delta\lambda = \frac{1}{2}$ in Eq. 9. The comparison of this figure with our Fig. 8 shows that even this rough method produces a correct estimate of the quantum deflection function with the exclusion of only one λ value. This value corresponds to a very large variation of $\arg S(\lambda)$ between two consecutive integer l values.

figure. By increasing f from 0.5 to 2.0, all the points tend to lie on the same curve in increasing ranges of b .

Comparing the behavior of the points representing $\Theta_Q(\lambda)$ with the corresponding ones for the real potential one observes that the imaginary part of the potential delays the approach of the classical limit. The addition of an imaginary part increases the non-homogeneity of the medium in which the particles propagate and favors the survival of wave effects.

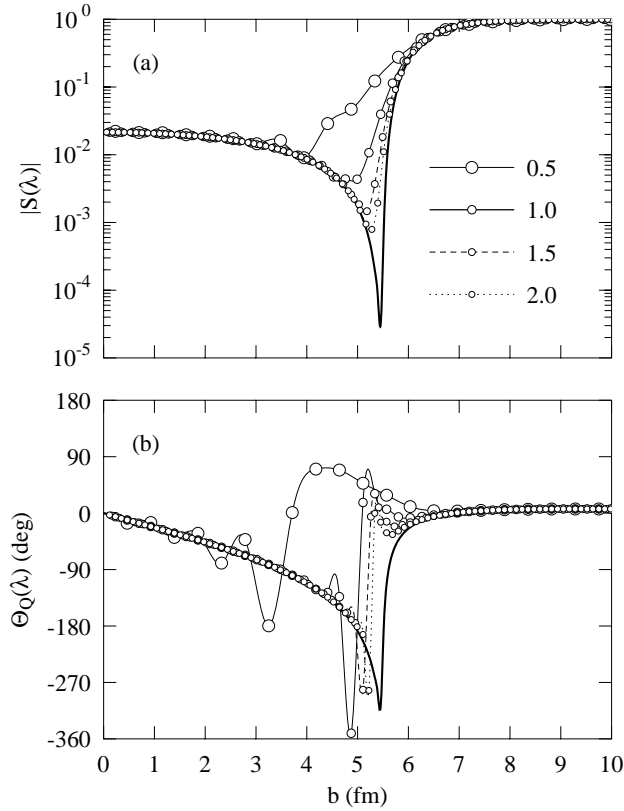


FIG. 10. The open dots give the moduli of the scattering functions (panel (a)) and the quantum deflection functions (panel (b)) calculated, for the 4 values of the \hbar reduction factor given in the figure, at half-integer and at $\lambda = bk$ values, respectively. The thick curves show the corresponding classical quantities and the other curves are the cubic spline interpolations of the dots.

It is interesting to observe that, for $f = 0.5$ and b larger than about 4 fm, $\Theta_Q(\lambda)$ has characteristics typical of a repulsive interaction. These are similar to those of the deflection function of the barrier term of the Brink and Takigawa approximation, which accounts for the contribution from the reflection phenomenon of the incoming waves in the region of rapid variation of the properties of the interaction.

The variations with f of the full, near- and far-side cross sections are shown in Figs. 11, 12, and 13, respectively.

In these figures the curves corresponding to the values of f from 0.5 to 2.0 are rather far from having common

envelopes. In the backward hemisphere and for the full and far-side cross sections, these common envelopes only begin to appear for the curves with $f = 1.5$ and 2.0. On the contrary, the existence of a well defined interference region is clearly shown by the calculations with values of f from 3.0 to 4.0, given in insets (b).

Thanks to the rapid decrease of the near-side cross section, by decreasing the angle below 180° , the boundaries of the interference region are far better defined for the complex potential full cross section than for the real potential one. The addition of the imaginary part to the optical potential has strongly increased the average slope of the backward near-side cross section and has considerably reduced, or perhaps eliminated, the long period oscillations appearing in the inset (b) of Fig. 9. Both these facts contribute to a better definition of the interference region for the complex optical potential full cross section.

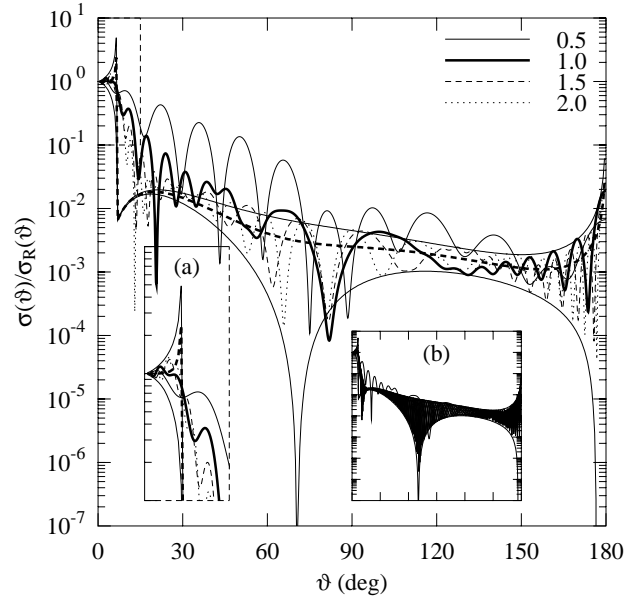


FIG. 11. The same as Fig. 5 for the full cross sections of the complex optical potential at $E_{\text{Lab}} = 132$ MeV.

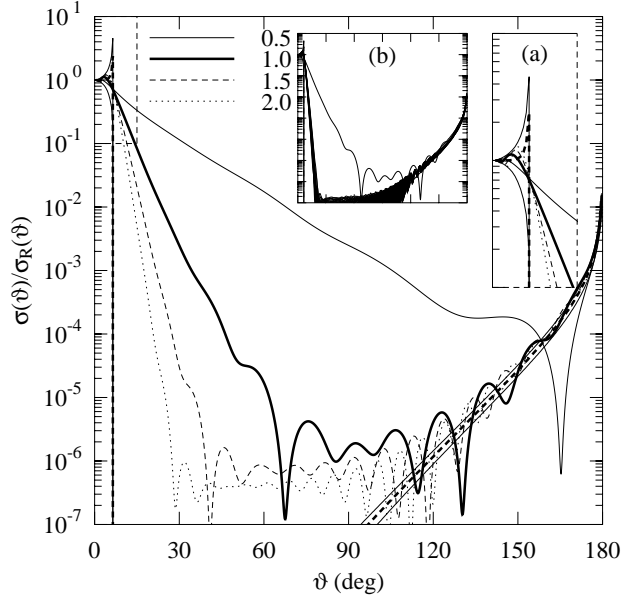


FIG. 12. The same as Fig. 5 for the near-side cross sections of the complex optical potential at $E_{\text{Lab}} = 132$ MeV.

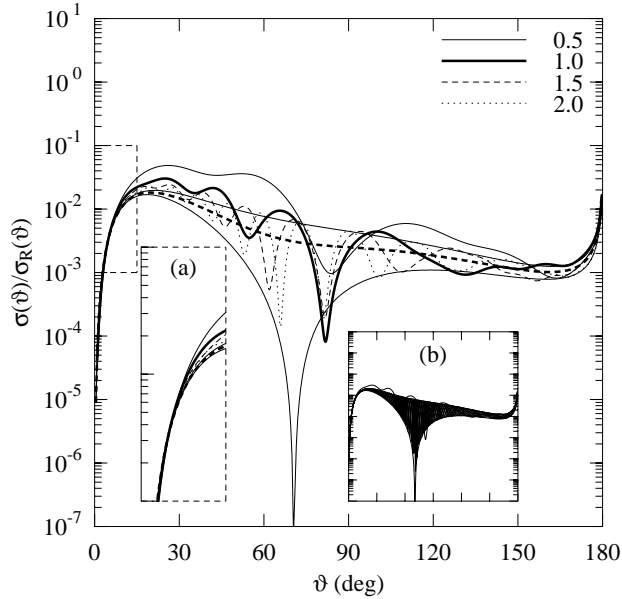


FIG. 13. The same as Fig. 5 for the near-side cross sections of the complex optical potential at $E_{\text{Lab}} = 132$ MeV.

The interference region, obtained using a pure quantum calculation, is just the one previously calculated using the classical mechanics. This shows that the analysis of the nature of the different contributions to the cross section can be done in absence of any classical mechanics calculation.

The presence of at least one classical-like contribution in the far-side cross section is proved by the behavior of the cross section at backward angles, and by its continuation, passing through the glory singularity, in the near-side cross section at backward angle. At forward angles,

the violation of the interference limits confirms the non-classical origin of the other contribution, responsible for the oscillatory pattern in the far-side cross section.

In the classical near-side shadow region, the existence of an approximately constant contribution to the quantum cross section is clearly displayed by the dashed and dotted curves of Fig. 12. This is the contribution which is responsible for the appearance of oscillations around the exponential drop of the near-side cross section at the right of θ_C , and around the classical-like contribution in the backward hemisphere. We did not attempt to investigate whether this contribution arises from some physical fact or from the numerical procedure used to calculate the cross sections.

V. COMPLEX OPTICAL POTENTIAL CROSS SECTION: $E_{\text{LAB}} = 200$ MEV

The second complex optical potential considered is one of the potentials whose cross section fits the experimental data at $E_{\text{Lab}} = 200$ MeV [4]. This potential also has conventional Woods-Saxon form factors with parameters $V_0 = 216.3$ MeV, $R_v = 3.2847$ fm, $d_v = 0.927$ fm, for the real part, and $W_0 = 17.83$ MeV, $R_w = 5.8625$ fm, and $d_w = 0.541$ fm for the imaginary part.

This case was considered because an analysis similar to that of Ref. [10] shows that the semiclassical Brink and Takigawa method fails to reproduce quantitatively the optical cross section in the whole angular range.

The results of the semiclassical analysis are summarized in Fig. 14, where the medium and heavy solid lines show the full semiclassical and the exact cross sections, respectively, while the thin solid and dashed lines show the barrier and the internal cross sections. In the inset (a) the corresponding far-side cross sections are shown.

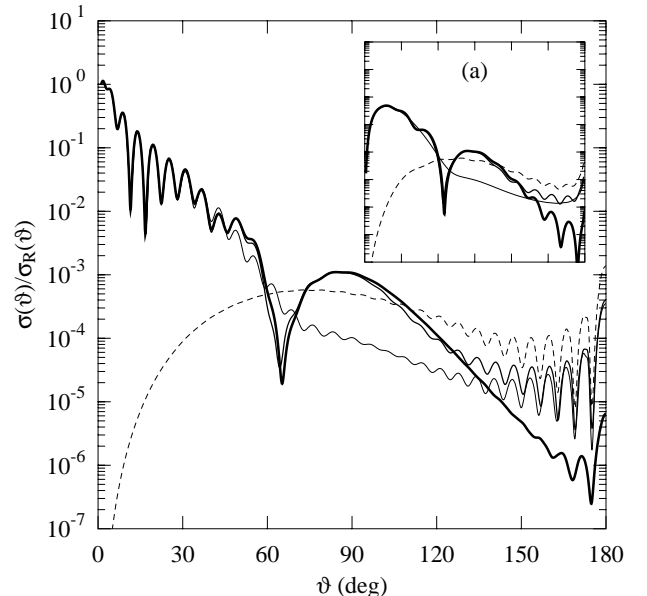


FIG. 14. Full semiclassical (medium thick line) and quantum cross sections (heavy thick line) for the $E_{\text{Lab}} = 200$ MeV case, together with the barrier (thin solid line) and the internal (thin dashed line) cross sections. Using the same lines, in the inset (a) the corresponding far-side cross sections are shown.

The agreement between the semiclassical and the exact cross sections is rather good only for scattering angles smaller than about 120° . As for the 132 MeV case, in this region the oscillations appearing in the exact far-side cross section can be explained as arising from the interference between far-side contributions from the barrier and the internal amplitudes. This casts doubts on the appropriateness of the use of the Airy terminology for the interference pattern for the 200 MeV potential.

At angles larger than 120° , however, the semiclassical and the exact cross sections are in large disagreement and this disagreement suggests caution in attributing a physical meaning to the semiclassical analysis.

The reason of the failure of the Brink and Takigawa approximation is probably connected with the fact that the case here considered is outside the range of applicability of the method. For this potential the complex orbiting angular momentum at which the barrier turning points coalesce is far from the real λ axis. On the contrary a different orbiting angular momentum is very close to the physical region. This is the angular momentum at which the internal turning point coalesces with a turning point different from those usually considered in the Brink and Takigawa approximation. This orbiting point, not treated correctly by the approximation, may be responsible for the anomalous behavior of the semiclassical cross sections.

The hope is that the present recipe can provide some useful and more clear indications on the nature of the amplitudes contributing to the cross section of this potential.

A. Comparison with the classical cross section

In Fig. 15 the classical $\Theta(\lambda)$ and $\sqrt{P(\lambda)}$ are shown together with the corresponding quantum quantities. With respect to the 132 MeV case, the minimum of the deflection function corresponding to the nuclear rainbow has moved to a deflection angle $\Theta_n \simeq -125^\circ$.

Because the nuclear rainbow singularity slides [12] toward a deflection angle larger than -180° , the backward glory singularities are suppressed, and only four branches of the deflection function contribute to the cross section. The panels of Fig. 16 show that, in this case, the regions to the right of the Coulomb rainbow θ_C (for the near-side cross section) and to the right of the nuclear rainbow θ_n (for the far-side and the full cross sections) are classical shadow regions.

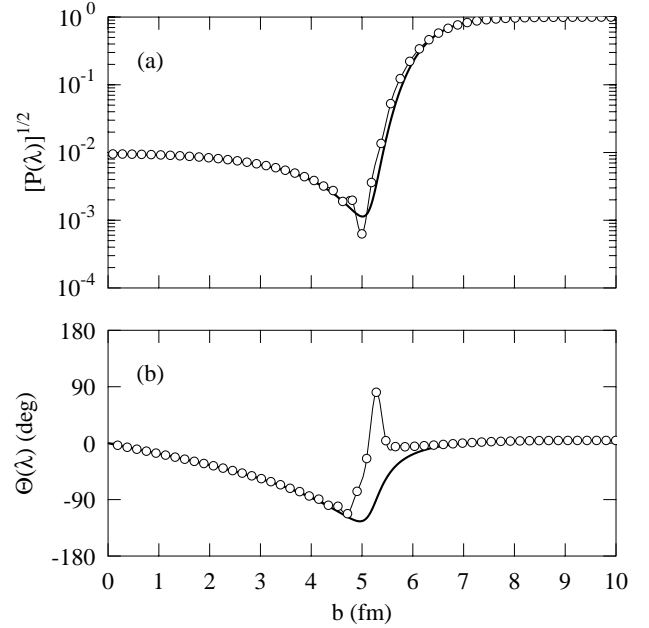


FIG. 15. The same as Fig. 8 for the complex optical potential at $E_{\text{Lab}} = 200$ MeV.

The quantities $\Theta_Q(\lambda)$ and $|S(\lambda)|$ are in substantial agreement with the corresponding classical ones in b ranges wider than for the 132 MeV case. However, the violations of the interference limits of the quantum full and far-side cross sections, shown in the panels (b) and (d) of Fig.16, are not smaller than in the lower energy case. For angles smaller than about 60° the far-side quantum cross section is largely outside of the classical interference region. This suggests that also for this potential, as for the 132 MeV case, these oscillations cannot be interpreted as arising from the interference between two classical-like contributions.

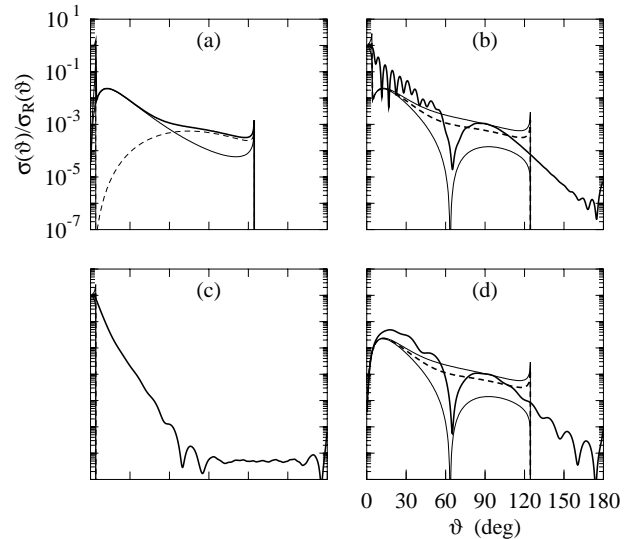


FIG. 16. The same as Fig. 2 for the complex optical potential at $E_{\text{Lab}} = 200$ MeV.

In panel (c) of Fig. 16 we clearly see the contribution from an almost constant additional term, which interferes with the exponential-like decrease of the cross section to the right of θ_C . It is more evident than in the corresponding panel of Fig. 9, where its presence was barely apparent, in the backward hemisphere, through its interference with the near-side classical-like contribution in this region.

B. Pure quantum analysis

For the 200 MeV potential, the figures from 17 to 20 correspond to the figures from 10 to 13, for the 132 MeV case. By comparing Fig. 17 with Fig. 10 one observes that, by decreasing \hbar , the properties of $S(\lambda)$ approach of the classical limit faster in the higher energy case. This is true also for the properties of the cross sections, and depends on the fact that for the higher energy the wavelength is smaller. In particular, by looking at Fig. 18 and Fig. 20 one observes that the quantum curves begin to have as upper and lower envelopes the interference limits, for scattering angles around 60° , already with a \hbar reducing factor of 1.5. From this value upward the interference pattern, below the classical nuclear rainbow angle, can be considered a genuine Airy-like pattern.

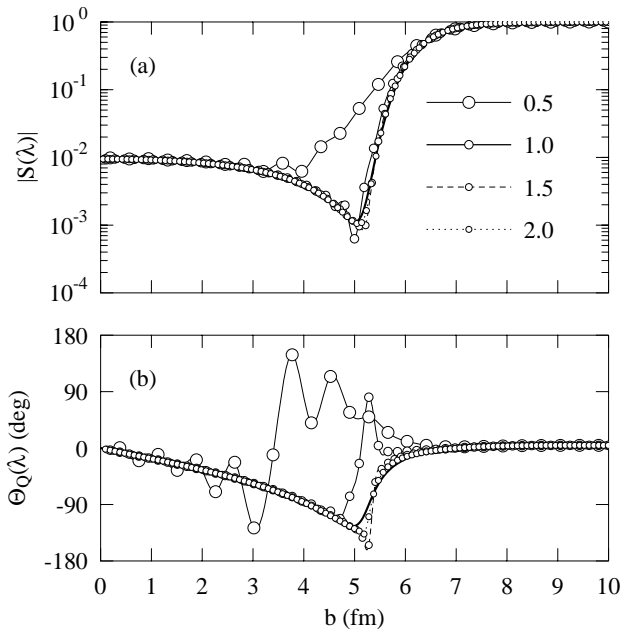


FIG. 17. The same as Fig. 10 for the complex optical potential at $E_{\text{Lab}} = 200$ MeV.

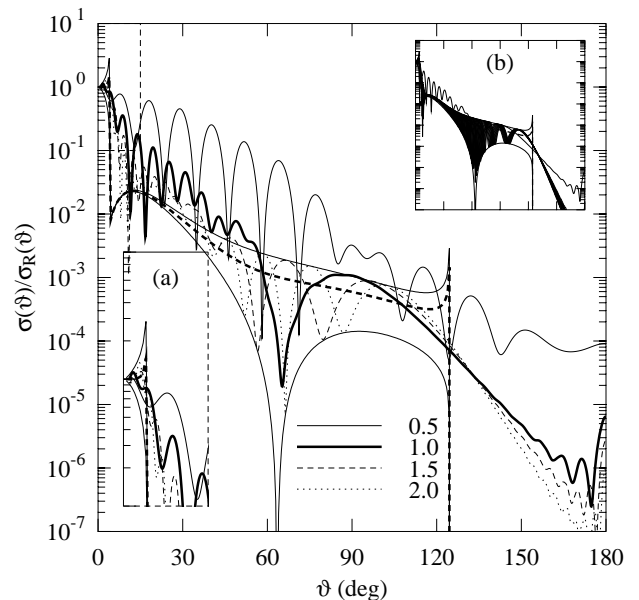


FIG. 18. The same as Fig. 5 for the full cross sections of the complex optical potential at $E_{\text{Lab}} = 200$ MeV.

In the inset (b) of Figs. 18 and 20, one again observes that the quantum calculations with f values ranging from 3.0 to 4.0, very well define the classical interference region, apart from problems connected with the quantum illumination of the classical shadow regions. Also in this case, the good definition of the interference region allows one to test the classical origin of the different amplitudes contributing to the quantum cross section by using only the calculations of a standard optical potential code.

In the forward hemisphere, the values of the true far-side cross section largely violates the classical interference limits. This confirms the inappropriateness of using the rainbow terminology for the interference patterns appearing in this and in the full cross sections.

VI. CONCLUSIONS

The simple recipe of shrinking \hbar , in a conventional optical potential calculation, provides useful information on the nature of the different amplitudes contributing to the cross section.

By decreasing \hbar the different characteristics of the cross section smoothly change, with different rapidity. In the major part of the angular interval, below some \hbar value, no further changes are observed in the cross sections with decreasing \hbar , apart from the sliding of the interference pattern within well defined regions, with an increasing number of oscillations. These are the characteristics connected with the realization of the transition from the dynamical regime governed by the quantum mechanics rules to that governed by classical mechanics ones.

The recipe can be easily implemented in any optical potential code, providing a practical tool for a rapid check of the classical properties of the cross section of a given potential.

The possibility of producing optical potential cross sections, attributing different values to \hbar , can also be used as a laboratory which provides useful cross sections for testing the effectiveness of the semiclassical techniques currently used.

As one example of the tests that could be performed let us consider the 132 MeV case. Following the Brink and Takigawa approximation, in this case the oscillations appearing in the far side cross section arise from the interference between the far-side contributions to the barrier and the internal amplitudes [10]. A similar result has also been obtained [13,14] (with an approximate calculation [15] of the barrier and internal amplitudes) for the same and for several other optical potentials used to describe the elastic scattering of light heavy-ions. The results obtained in all these cases show that the barrier far-side contribution is responsible for the Fraunhofer-like pattern appearing in the barrier cross section, and this strongly suggests that it must be regarded as a diffractive contribution.

The present analysis shows that by decreasing the value of \hbar this contribution smoothly changes, until it assumes a form which must be identified with the contribution from classical-like far-side trajectories.

In the Brink and Takigawa approximation the contribution from these trajectories should be contained in the internal term, and this implies that a critical \hbar range exists in which the contribution migrates from the barrier to the internal term. This migration is probably connected with the change of the characteristics of the trajectories described in the complex r plane by the turning points of the radial equation.

In this critical region, detailed semiclassical analyses of the cross sections could provide interesting information on the validity, or on the limits, of the semiclassical techniques, and allow us to achieve a better understanding

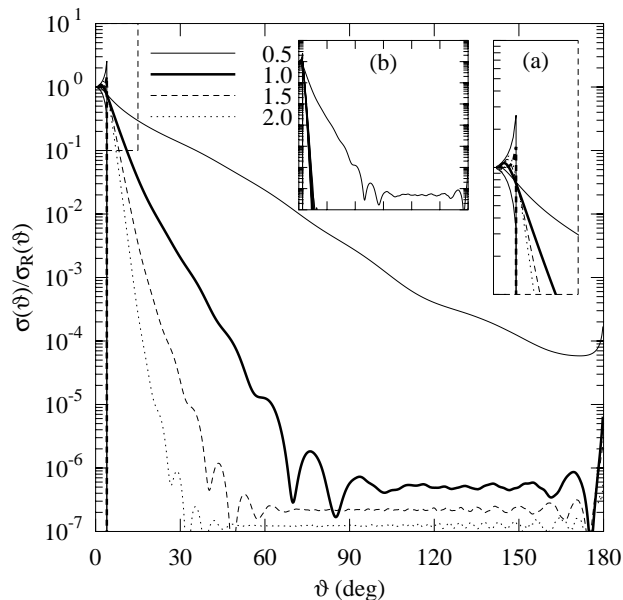


FIG. 19. The same as Fig. 5 for the near-side cross sections of the complex optical potential at $E_{\text{Lab}} = 200$ MeV.

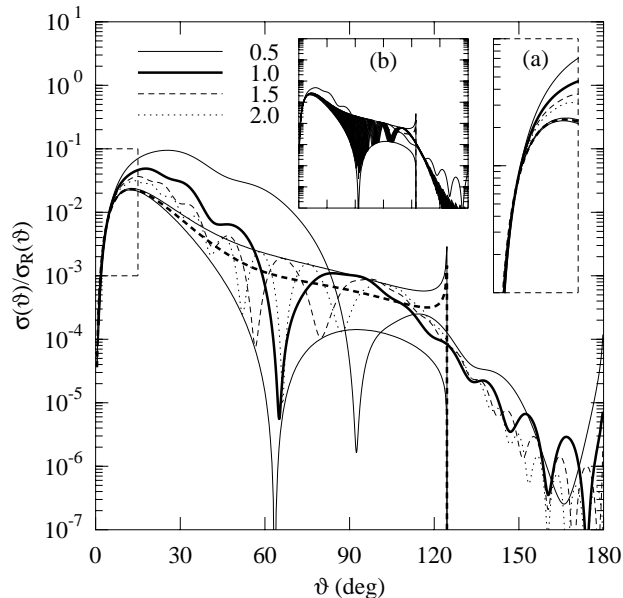


FIG. 20. The same as Fig. 5 for the far-side cross sections of the complex optical potential at $E_{\text{Lab}} = 200$ MeV.

Figure 19 shows that, as in the previous case, the behavior of the near-side cross section in the classical shadow region is largely responsible for the violation of the interference limits of the full cross section.

In the inset (b) of the same figure one can observe that, for f values from 3.0 to 4.0 and for $\theta > \theta_C$, the almost constant contribution to the near-side cross section is outside the plotted area. Only the rapidly decreasing exponential contribution appears in a restricted angular range above θ_C .

of the transition between the quantum and the classical regimes.

- [1] Dao T. Khoa, W. von Oertzen, H. G. Bohlen, and F. Nuoffer, Nucl. Phys. **A672**, 387 (2000).
- [2] M. P. Nicoli, F. Haas, S. Szilner, Z. Basrak, A. Morsad, G. R. Satchler, and M. E. Brandan, Phys. Rev. C **61**, 034609 (2000).
- [3] M. P. Nicoli, F. Haas, R. M. Freeman, N. Aissaoui, C. Beck, A. Elanique, R. Nouicer, S. Szilner, Z. Basrak, A. Morsad, M. E. Brandan, and G. R. Satchler, Phys. Rev. C **60**, 064608 (2000).
- [4] A. A. Ogloblin, Yu. A. Glukhov, W. H. Trzaska, A. S. Dem'yanova, S. A. Goncharov, R. Julin, S. V. Klebnikov, M. Mutterer, M. V. Rozhkov, V. P. Rudakov, G. P. Tiorin, Dao T. Khoa, and G. R. Satchler, Phys. Rev. C **62**, 044601 (2000).
- [5] K. W. Ford, and J. A. Wheeler, Ann. Phys. (N.Y.) **7**, 259 (1959)
- [6] D. M. Brink, *Semi-Classical Methods for Nucleus-Nucleus Scattering* (Cambridge University Press), 1985.
- [7] D. M. Brink, *Semi-Classical Methods for Nucleus-Nucleus Scattering* (Cambridge University Press), 1985, p.7, 49.
- [8] R. Broglia, S. Landowne, R. A. Malfliet, V. Rostokin and Aa. Winther, Phys. Rep., Phys. Lett. **11C**, 1 (1974).
- [9] R. C. Fuller, Phys. Rev. C **12**, 1561 (1975).
- [10] R. Anni, Phys. Rev. C **63**, 031601 (2001).
- [11] D. Brink and N. Takigawa, Nucl. Phys. **A279**, 159 (1977).
- [12] K.M. McVoy, Nucl. Phys. **A 455**, 141, (1986).
- [13] F. Michel, F. Brau, G.Reidemeister, and S. Ohkubo, Phys. Rev. Lett. **85** 1823 (2000).
- [14] F. Michel, G.Reidemeister, and S. Ohkubo, Phys. Rev. C **63**, 0346XX (2001).
- [15] J. Albiński and F. Michel, Phys. Rev. C **25** 213 (1982).